Effects of Methods of Manufacturing Sputtering Targets on Characteristics of Coatings

J.J. Finley and S.D. Walck, PPG Glass Technology Center, PPG Industries, Inc., Pittsburgh, PA; and E. Bono, Crucible Research, A Division of Crucible Materials Corporation, Pittsburgh, PA

Key Words: Sputtering target, Sputter deposition, TiAl, Coating

ABSTRACT

This paper compares the effect that different methods of manufacturing sputtering targets have on coatings. Targets of the same binary metallic alloy were produced by casting and powder metallurgy and sputtered to produce alloy coatings. Composition of the alloy coating was determined by X-ray fluorescence measurements as a function of the target depth, thus simulating behavior with target wear. Microstructure of the target surface was examined before and after sputtering, and correlation to the coating composition was determined. Other factors, such as sputtering and uniformity of the alloy targets, were compared.

INTRODUCTION

Precise composition and morphology of sputtering target material is of utmost importance for coated product performance. Target morphology and composition can influence sputtering rates, coating composition and uniformity [1]. Target compositions that differ from the specified composition can quickly lead to costly product or process problems. For example, multilayer stacks for optical filter applications depend critically on precise refractive indices of the target materials. The field behavior of commercial products is compromised if the composition is contaminated with easily corrodible materials, and the thermal stability of functional coatings, such as low emissivity coatings, are degraded if the correct thicknesses and compositions of the layers are not controlled [2]. Reactive sputtering to produce aesthetic coatings for decorative purposes, or transparent conductive oxides for display technology depend on the correct stoichiometry. Changes in coating uniformity or composition, or drift in sputtering rate as a result of target morphology or composition are simply not acceptable for a viable product or process.

In this paper, the differences between alloy targets with the same binary metallic alloy, but produced by two different methods were examined. Specifically, targets produced by casting and hot isostatic pressing (HIP'ing) of pre-alloyed powder of TiAl were chosen for comparison. The elemental components of this alloy are different in their physical properties, e.g., mass, density, electrical and thermal conductivity, and melting point. In addition, the processes used to fabricate the sputtering targets are fundamentally different. An understanding of the behavior of these cathode targets, and the coatings produced by these targets, is critical for industrial applications, as detailed above.

For this investigation, the morphology of these targets and the sputtered film produced from the targets were examined in detail. The physical properties of the coatings were measured and compared. The sputtering process, combined with various measurement techniques, was used as an analytical, rather than a production tool, to explore target materials and sputtered coatings. Coating compositions were determined using Secondary Neutral Mass Spectrometry (SNMS) depth profiling, and X-ray fluorescence (XRF) analysis. Coating thicknesses were measured using a stylus profilometer. Coating densities and sputtering rates were calculated from these measurements. The resistivities of the coatings were determined from sheet resistance and thickness measurement. The sheet resistance was measured using a four-point probe measurement. Coating structure and morphology were determined using both X-ray diffraction (XRD) and electron diffraction, and transmission electron microscopy (TEM). The morphology of the target surface was examined using optical microscopy and X-ray diffraction, and the structure was determined using XRD.

EXPERIMENT

Cathode Targets

In the DC magnetron sputtering process, the surface of a planar target is eroded to form the well known racetrack pattern, as shown in Figure 1. This pattern encircles the target surface where the erosion is greatest at the center and decreases towards the edge of the racetrack. Any physical or chemical change in the target as the target erodes could result in changes in sputtering rate, and possibly in composition and uniformity of the sputtered film.

 505/856-7188 ISSN 0737-5921

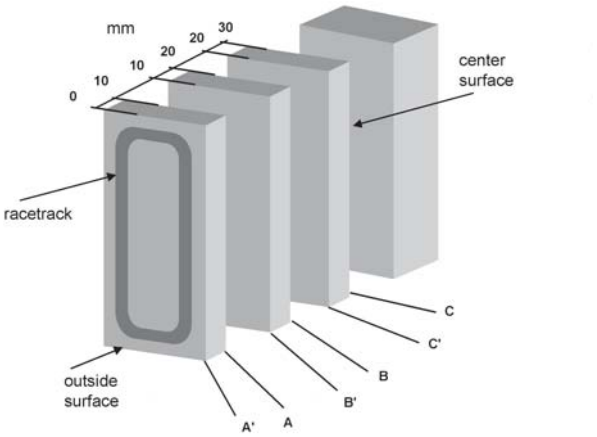

Figure 1: Schematic of the cross-section of a casting showing the racetrack, the location of each target plate in mm, and labels for each surface of the target plates.

HIP'ed targets have a fine isotropic microstructure and homogeneous composition [3], and it is assumed that the target composition is constant with wear. A cast target, on the other hand, exhibits different microstructural features through its cross-section consisting, in general, of the chill, columnar and equiaxed zones. In addition, compositional changes can be present due to coring segregation, which occurs due to the limitation of diffusion not allowing the solid to follow the solidus line in the phase diagram. Both the microstructure and composition variations in the cast structure depend on the difference in cooling rate from the surface (faster) to the interior of the casting during processing and any subsequent heat treatment.

To simulate the effect of the microstructural changes in the cast target on the properties of the coating as the target erodes, target plates were separated using a carbide tipped saw blade, as shown in Figure 2, and then reduced to their approximate thickness by milling with a carbide tipped cutter. The surface was ground flat on a wet surface grinder using a 36-grit aluminum oxide wheel. The target plates were labeled as shown in Figure 1.

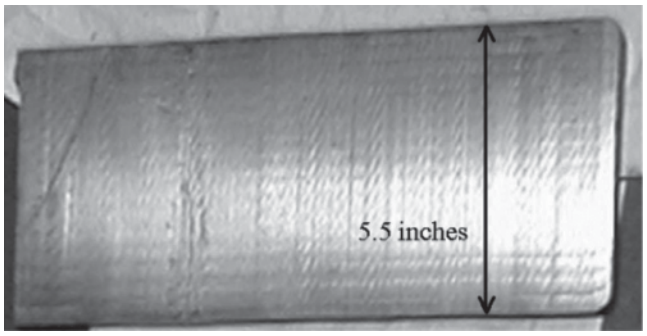

Figure 2. Unfinished surface of a TiAl target plate cut from a casting.

Plate A'A has outer surface A' located at 0.0 mm, and inner surface A at ~10 mm. The second plate from the outer plate, B'B, has surface B' at ~10 mm which is equivalent to surface A. The third plate, C'C, has surface C' at ~20 mm which is equivalent to surface B. Surface C at ~30 mm is located at the centerline of the casting. The locations of the surfaces in mm were derived from the sum of the approximate thicknesses of the finished targets; kerf loss due to cutting and grinding was ignored. Both surfaces of each plate were sputtered by flipping the targets.

The physical properties of the coatings were then determined as a function of the location of the surfaces in the casting. It was assumed that the composition of the HIP'ed target was constant with wear; therefore, only one surface was sputtered.

The HIP'ed target was made using pre-alloyed powders. The TiAl powders were manufactured by first melting TiAl alloy under argon gas in an induction skull furnace and gas atomized into powder [4]. This process guarantees that each particle of metal has the same composition. The induction skull melting process is a refractory-free process that allows the molten alloy to be contained within a self-generating thin solid shell of the same composition.

The HIP'ed target was fabricated by loading the pre-alloyed powder into a metal container that was subsequently evacuated and sealed. The container was then placed into a high-pressure vessel under 15 kpsi of argon at 1090°C. This step bonds the particles together by diffusion, leaving a fully dense solid of uniform composition.

The cast target was fabricated by induction skull melting the raw metals (titanium and aluminum), and pouring the melt into a graphite mold for casting. The casting dimensions were approximately 5.5" (the width of the targets), 10" height (the length of the targets) and 3.25" to accommodate the thickness of the 6six half targets cut from the casting (see Figure 2).

The microstructure of the target surface was examined using optical metallography and the composition of the target was determined using chemical analysis and XRD. Metallurgical samples were polished and examined under polarized light at 50 X magnification. The cross-section of the three targets cut from the casting, and the HIP'ed target were etched with a solution of 15% nitric acid and 1% hydrofluoric acid, and photographed to show the overall distribution of structures in the targets. The sputter etched targets were photographed to illustrate the microstructural features.

XRD patterns of the powder samples ground from the cast and HIP'ed targets were used to identify the phases using the JCPDS database [5] and to determine the lattice parameters. The samples were run on a Philips X'Pert-MDP diffractometer equipped with a curved graphite monochromator and Cu-Kα radiation, using the conventional θ/2θ Bragg-Brentano configuration.

DC Magnetron Sputtering

An ILS 1600 Airco (Von Ardenne Coating Technology) coater, installed with planar DC magnetron cathodes, and connected to a Advanced Energy Pinnacle® 10 kW power supply was used to deposit the coatings. The power supply was run in the constant power mode. To simplify analysis by avoiding the complications due to reactive sputtering, the target was sputtered in the metal mode in an argon gas atmosphere.

The targets were fixed to a 5-inch x 17-inch copper backing plate and mounted on a water cooled cathode block. It was necessary to distribute the targets among three cathode blocks; therefore, the samples were run over the period of several pumpdowns. The deposition took place at ambient temperature. The base pressure of the coater before deposition was less than 10^{-6} torr (0.13 mPa). Targets were conditioned by pre-sputtering for 15 minutes at 1.0 kW, in ultra high purity (99.999%) argon, with a flow rate of 100 sccm, and a pressure of 4 mtorr (0.53 Pa) before deposition. This insured removal of surface oxides and contaminants, and steady state deposition of the alloy. The cathode voltages ranged from 400 to 450 volts at 1.0 kW, just prior to deposition. A 2.3 mm thick clear float glass substrate was then transported into the vacuum chamber and coated by passing the substrate under the target at a line speed of 120 inches per minute.

Coating Properties

To determine the coating properties, three samples were deposited for each target surface of the cast target, and a single surface of the HIP'ed target, by passing a 12-inch square glass substrate under the target 20 times to deposit the coating. The power supply was set at 1.0 kW. Samples were taken from within 5 inches of the center of the substrate to insure coating uniformity. XRF, DC Plasma (DCP) analysis, thickness, and sheet resistance measurements were made on the samples, and the average and standard error of the data for the three samples were found. These data were used to calculate the sputter deposition rate, composition, density and resistivity of the coatings. TEM and XRD samples were measured to identify coating structure. Substrates for the TEM samples were affixed to the glass substrate prior to deposition, and an additional set of samples was run with three passes under the target.

Coating composition was determined from XRF measurements of 3.5 cm square samples. The concentration of the coating in micrograms per cm^2 ($\mu g/cm^2$) was measured, and the weight percent of aluminum and titanium was calculated. Small corrections to the Al and Ti concentrations obtained by XRF were required (< 0.1%) because of their content in the glass substrate. DCP analysis of representative coatings was used to calibrate the XRF measurements.

Coating thickness was measured using a Tencor Model P1 Long Scan Profiler. Prior to deposition, a deletion line was applied to the glass with a fine point permanent marker. After deposition, the line was removed with acetone and the stylus was scanned across the deleted area.

Sheet resistance was measured using an Alessi four point probe, and a Kiethley Model 196 digital multimeter. The film resistivity was determined from the thickness and *ex situ* measurements of sheet resistance, and using the equation, $\rho = R_s * t * 10^6$, where ρ is the resistivity in μohm-cm, R_s is the sheet resistance in ohms/square, and t is the coating thickness in cm.

For consistency, the sputtering rate was expressed in terms of thickness per pass for a cathode power of 1.0 kW, or Ångstroms per kilowatt-pass (Å/kW-pass). Coating density in g/cm^3 was calculated by dividing the concentration by the coating thickness.

XRD measurements of the coatings were run on the Philips X'Pert MDD Diffractometer and a parallel beam collimator on the detector, and employing glancing angle mode using a fixed incident angle of 1.0°. XRD patterns were used to identify the phases using the JCPDS database [5] and to determine the lattice parameters.

Coating structure was identified using transmission electron microscopy (TEM) samples made by depositing coatings on carbon coated support films on 200 mesh copper grids, and thin, freshly cleaved NaCl crystals, that were affixed to the glass substrate. Because thinner coatings were desired for TEM, the samples were coated with three passes under the target at 3.0 kW for a thickness of 500 Å. All other coater parameters remained constant. TEM samples were examined in a JEOL 200FX TEM and a Technai 20 Field-Emission TEM to determine the morphology of the coating and to identify any phases that may not have been resolved by X-ray diffraction (XRD).

Deposition Rate vs. Time

To determine the effect of sputtering time on the deposition rate, the target was sputtered over a period of up to six hours. This further enhances the effect of erosion on the grain structure as the target surface is sputtered etched. A sample was run initially (t = 0), and then for each subsequent hour. The cast target (surface C, see Figure 1) and HIP'ed target, representing the extremes in grain size, were compared. The targets were run in the same cathode block to eliminate any small variations that exist between blocks (i.e. magnetic field, gas flows). The coatings were deposited by passing the substrate under the target 10 times. All other coater parameters were kept constant.

Coating Composition and Thickness vs. Deposition Angle
To measure the variation in coating thickness and composition as a function of angle from the target surface, a 3.50 cm long substrate was positioned under the cathode and coated for 30 seconds at a power of 1.0 kW. The center of the substrate was positioned under the centerline of the target, i.e., midway between the erosion grooves. Samples from the cast target surface, C, and the HIP'ed target were compared. Ten-3.5 cm square samples were cut along the length of the substrate. The concentration of coating was measured for each sample using XRF values, and the coating density was used to calculate the thickness.

EXPERIMENT RESULTS

Cathode Targets
The microstructures of the targets are shown in Figures 3, 4, 5 and 6.

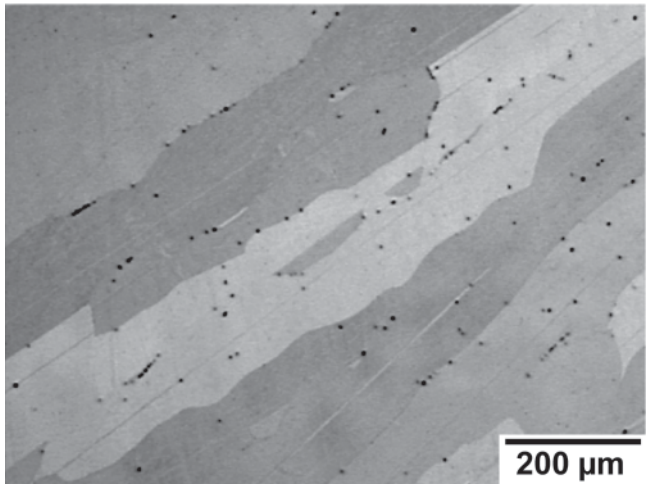

a.

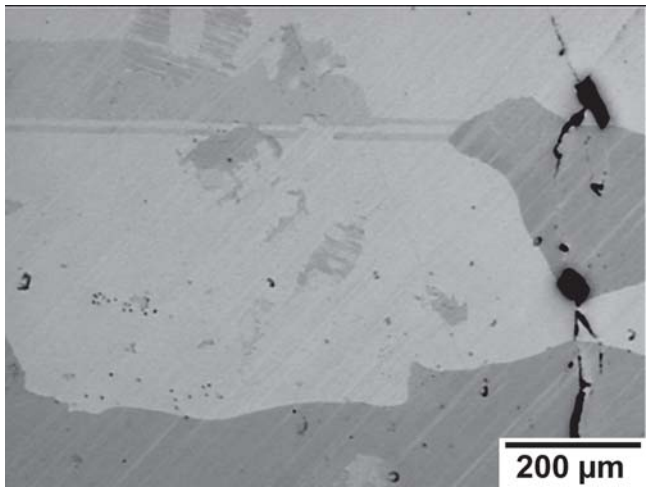

b.

Figure 3: TiAl cast target optical micrographs of (a) edge and (b) center.

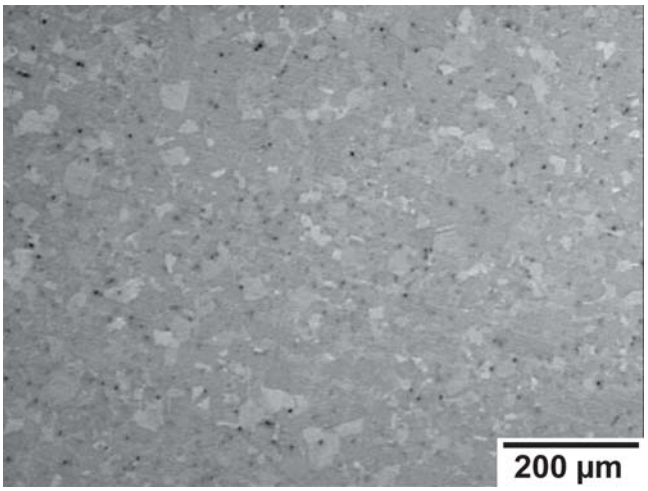

a.

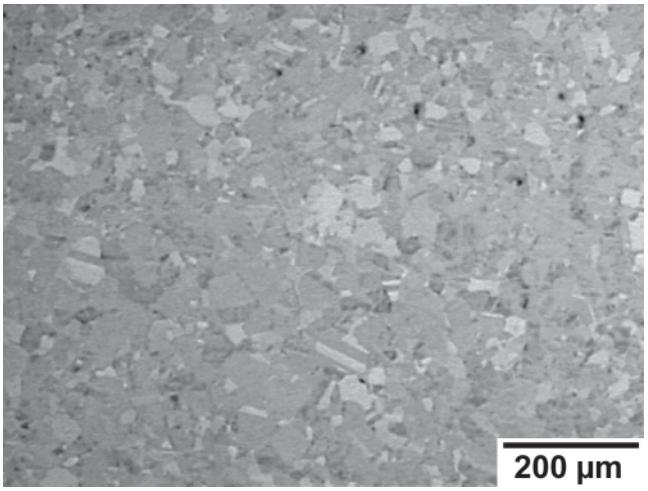

b.

Figure 4: TiAl HIP'ed target optical micrograph of the (a) edge and (b) center.

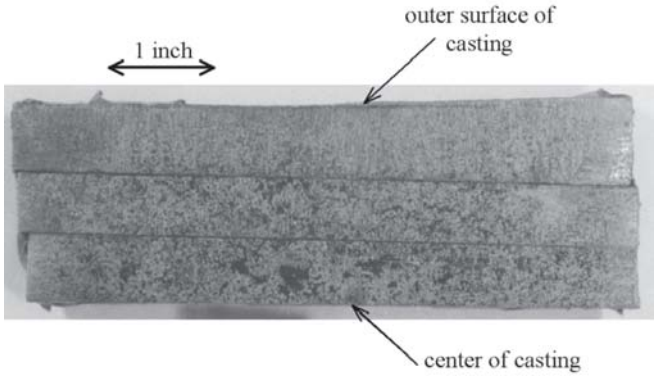

a.

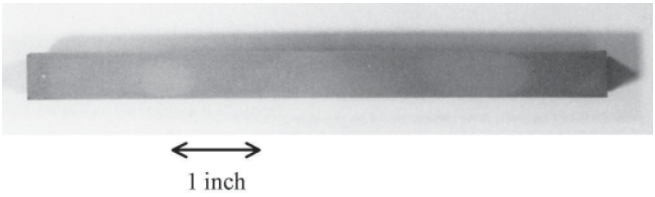

b.

Figure 5: TiAl macrophotographs of cross-section of the (a) cut cast and (b) HIP'ed targets.

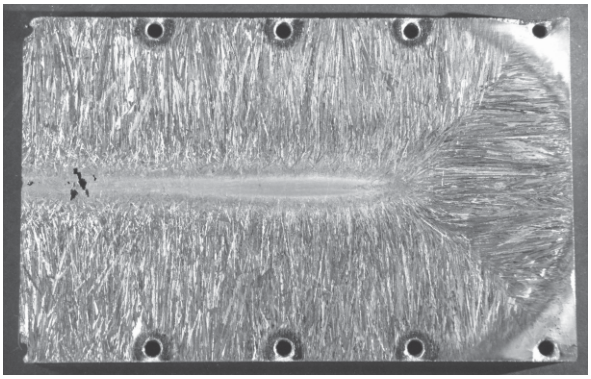

a.

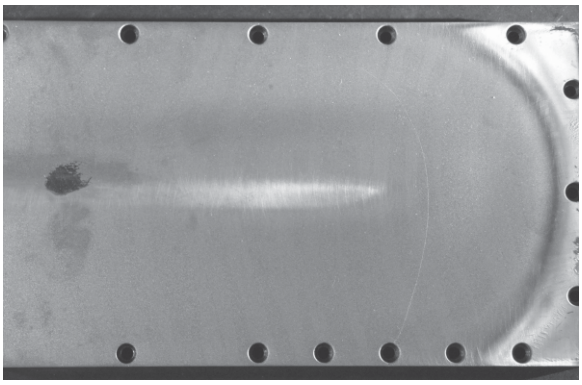

b.

Figure 6: Macrophotographs of the sputter etched surface of the (a) cast target (surface C), and the (b) HIP'ed target.

The microstructure of the cast targets exhibits the classical variations of a casting. The grains near the center of the casting are coarser than those at the edge, as shown in the micrographs in Figure 3a and b. In the center of the casting, shrinkage porosity is also seen. The macrophotograph of the etched cross-section of half of the casting is shown in Figure 5a. The figure also shows the coarser structure at the center. These microstructural features on the surface of the target become significantly enhanced after the target is sputtered, as shown in Figure 6a. It is also interesting to note the columnar structures meet at a 45° angle at the corners of the cast target. Surface morphology between equivalent surfaces (A,B' and B,C') in the sputtered areas appeared similar, as was expected.

By contrast, the HIP'ed target exhibits a fine grain structure throughout the whole target, as exhibited in the micrographs of Figure 4a and 4b. The corresponding macrophotograph of the etched cross-section, as shown in Figure 5b, is virtually featureless. Similarly, the sputtered etched surface of the target is featureless, as shown in Figure 6b. XRD results from powder that was ground from HIP'ed targets confirmed γ-TiAl phase (JCPDS 05-0678), as shown in Figure 7. XRD of powder ground from the surfaces of each cast target agreed with the results of the HIP'ed target.

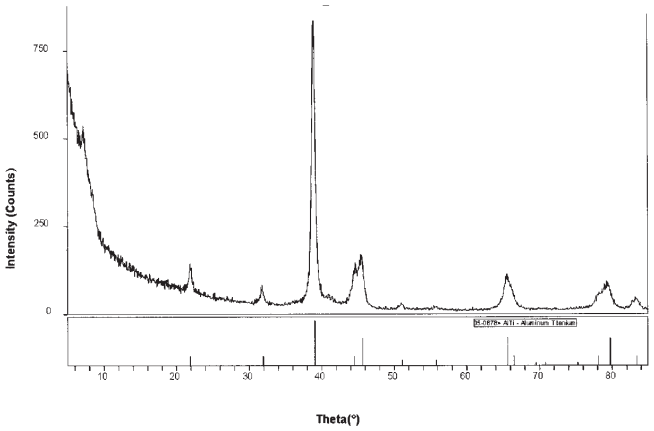

Figure 7: XRD powder diffraction pattern from powder ground from the HIP'ed target showing the γ-TiAl phase.

Chemical analysis of the pre-alloyed powder for the HIP'ed target yielded 36.5 wt % Al (50 at%). This agreed with the analysis of the HIP'ed block at the center and the edge. These two compositions were 36.17 and 36.4 wt % Al, respectively. Analysis of the cast target yielded 39.1 and 39.5 wt % Al at the edge and center, respectively. The margin of error in the measurement was ±0.25% wt %.

Coating Properties

Figure 8 shows the composition of the coating in wt % Al where each point represents the average composition of the three coated samples sputtered from one of the target surfaces of the cast target, as shown in Figure 2.

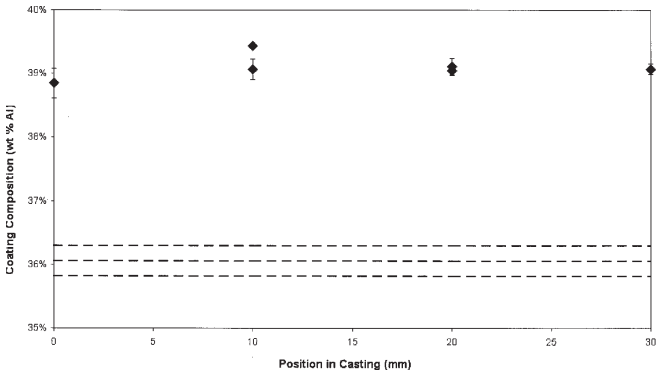

Figure 8: Al composition in wt % Al for coatings sputtered from surfaces of the cast (◆) and HIP'ed (---) targets as a function of position in the casting in mm.

The error bars represent the standard error of the mean. The average composition of the coating sputtered from the surface of the HIP'ed target is represented by the dotted line that extends the length of the x-axis (cross-section of the target). The dotted line denotes that the value at the surface of the target is continuous through the cross-section, since uniform properties through the cross-section of the target were assumed. The upper and lower lines represent the standard error of the mean.

The figure indicates that the individual values differ little through the cross-section of the casting. The data show the average values of the compositions of all the coatings from the cast target are 39.1 wt % Al (53.3 at % Al). The composition of the coatings is also in close agreement with the composition of the cast target. In comparison, the composition of the coating sputtered from the HIP'ed target has an average value of 36.1 wt % Al (50.1 atomic %). This is also in agreement with the value for the composition of the target.

Table 1 summarizes the compositions in wt % Al of the pre-alloyed powder, the target surfaces near the center and edge, and the average composition of the coating sputtered from the HIP'ed and cast target.

Table 1: Summary of compositions in wt% of Al of the starting materials, target and coating.

	Composition (wt% Al)			
Target	**Pre-Alloyed Powder**	**Center**	**Edge**	**Coating**
HIP'ed	36.5	36.2	36.4	36.1
Cast	-	39.1	39.5	39.1

The average sputtering rates are shown in Figure 9. The data vary between 57.4 and 58.9 Å/kW-pass, with an average of 57.4 for all the surfaces of the cast target, and 58.3 for the HIP'ed target. At a power of 1.0 kW, the coatings had a rate of 9Å /sec, and an average thickness of 1170 Å.

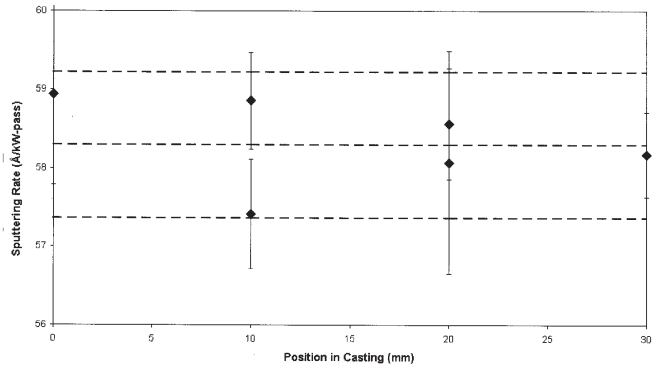

Figure 9: Average sputtering rate of TiAl in Å/kW-pass of the cast (◆) and HIP'ed (---) targets as a function of position in the casting in mm.

The data indicate that the differences between the average deposition rates of the cast and the HIP'ed targets are not statistically significant. The data points for the deposition rates for all the surfaces of the cast target fall within the error bars for the HIP'ed target sputtering rate.

The average densities of the coatings sputtered from the cast and HIP'ed targets are shown in Figure 10. The average density of the coating sputtered from the HIP'ed target is 3.56 g/cm^3, and is greater than the coating sputtered from the cast targets. The densities of the coatings sputtered from the cast targets range from 3.41 to 3.49 g/cm^3, with an average of 3.45 g/cm^3. The differences in densities among the coatings sputtered from the surfaces of the cast targets are statistically insignificant. The difference in density between the cast and HIP'ed targets is due to the differences in composition.

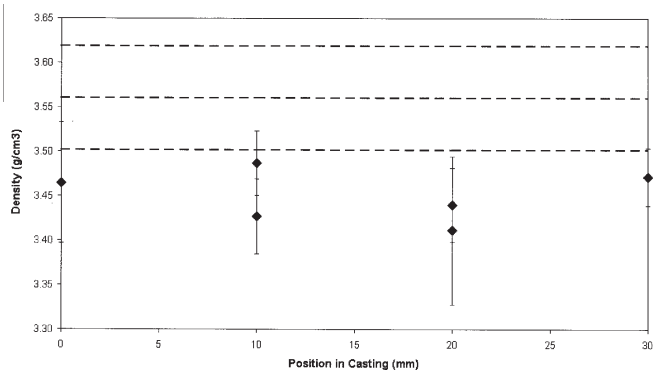

Figure 10: Density of the coatings in grams/cm^3 sputtered from the HIP'ed (---) and cast (◆) targets as a function of position in the casting in mm.

The resistivity values for the coatings sputtered from the cast and HIP'ed targets are shown in Figure 11.

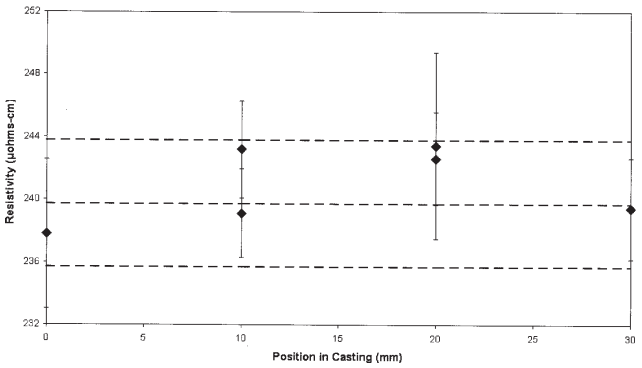

Figure 11: Resistivity in μohm-cm of the coatings sputtered from the HIP'ed (---) and cast (◆) targets as a function of position in the casting in mm.

Figure 11 shows the data for the coatings from the cast target with resistivity values ranging from 238 to 243 μohm-cm and an average value of 241 μohm-cm. The average value for the resistivity of the HIP'ed target is 240 μohm-cm. There is no statistically significant difference in resistivity for coatings deposited from any of the surfaces of the cast target, or between coatings deposited from the cast and the HIP'ed target.

Figure 12 shows the XRD patterns for the TiAl coatings sputtered from the HIP'ed and cast targets. The XRD patterns for all of the coatings from both the cast and HIP'ed targets are indistinguishable in their diffraction patterns. A broad amorphous peak is present 39.4° (Cu-Kα), indicating an amorphous structure. A broad amorphous peak from the glass substrate is also seen at a lower angle.

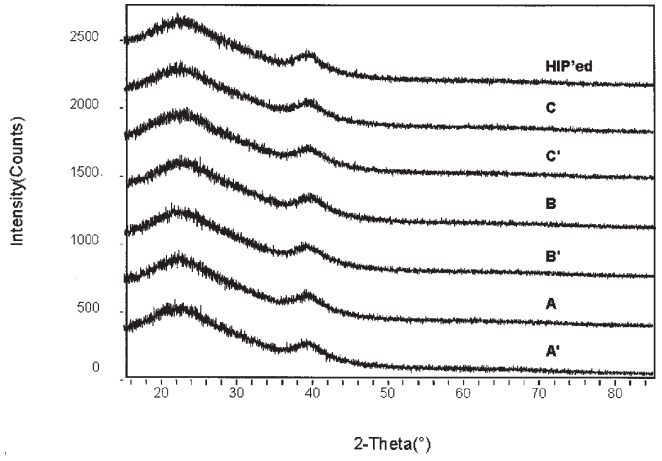

Figure 12: XRD of TiAl coatings sputtered from each surface of the HIP'ed and cast targets.

Selected area electron diffraction (SAED) patterns also show the corresponding amorphous ring. The TEM micrographs revealed a very fine morphology for the coatings grown on both the carbon support films and NaCl single crystals with no diffraction contrast seen. Figure 13 is a high resolution TEM (HREM) image of a 500 Å thick coating deposited from the HIP'ed target onto a NaCl substrate. Although amorphous, the coating shows evidence of short range order. Similar evidence was seen for the coating on the carbon support film

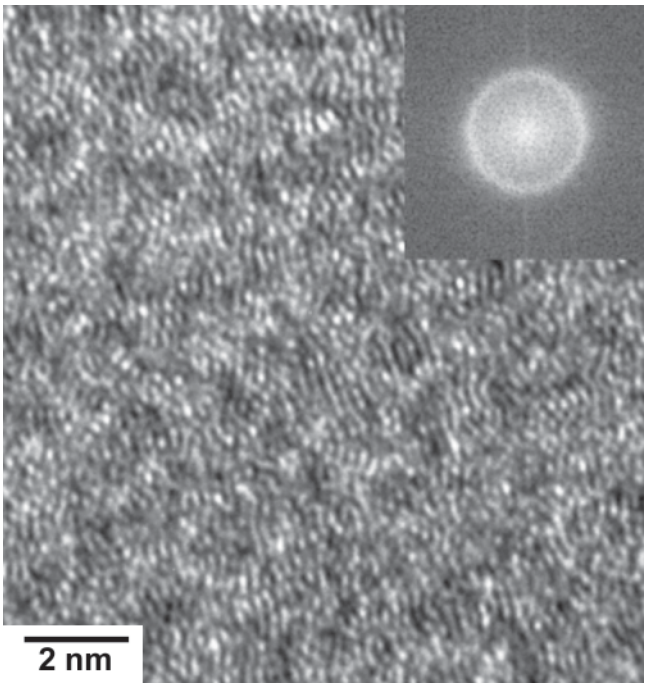

Figure 13: High resolution TEM (HREM) image of a 500 Å thick TiAl coating deposited from the HIP'ed target onto a NaCl substrate.

A summary of the sputtering rate and the properties of the coatings sputtered from the cast and HIP'ed targets are shown in Table 2.

Table 2: Summary of the coating properties for coatings sputtered from cast and HIP'ed targets.

Coating Properties (average values)					
Target	**Structure**	**Composition (wt % Al)**	**Density (g/cm^3)**	**Sputtering Rate (Å/kW-pass)**	**Resistivity (μohm-cm)**
HIP'ed	Amorphous	36.1	3.56	58.3	240
Cast	Amorphous	39.1	3.45	58.3	241

Sputtering Rate vs. Time

The graph in Figure 14 illustrates how the sputtering rate (a) and cathode voltage (b) change as a function of time for the HIP'ed and cast (surface C) targets.

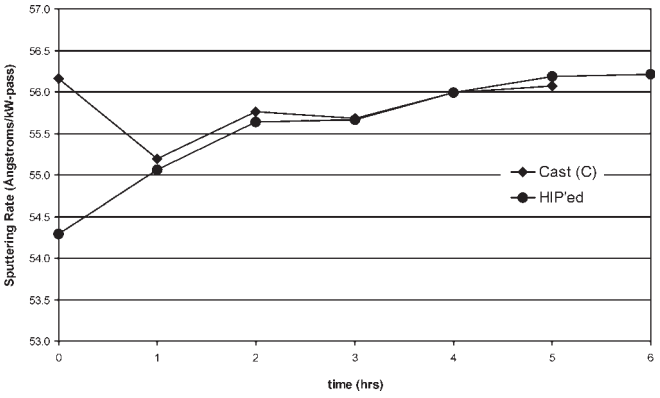

a.

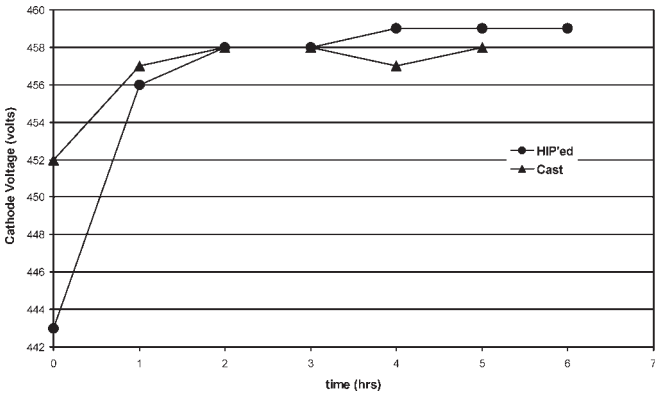

b.

Figure 14: Sputtering Rate in Ångstroms/kW-pass (a) and Cathode Voltage in volts (b) as a function of time in hours, for the HIP'ed and cast targets.

Initially, the voltage and sputtering rates were different, but were almost equal by the first hour. The change in both the sputtering rate and voltage over the time period were also approximately the same for both targets. The data illustrate that over this time period there was no marked difference in either the sputtering rate or voltage (at a constant cathode power) between the largest grain cast target and finest grain HIP'ed target surfaces.

Coating Composition and Thickness vs. Deposition Angle

Figure 15a shows the thickness of the coating normalized to the maximum thickness, and Figure 15b shows the weight % Al, as a function of position on the substrate. Figure 15c shows the normalized thickness as a function of the angle θ, where θ is the angle between the target normal at the midpoint between the racetracks, and the line from the target to a point on the substrate, as shown in Figure 16. The midpoint is located at 0, and the point on the substrate is located at p. The coatings were deposited from the HIP'ed target, and the cast target (surface C) onto stationary substrates.

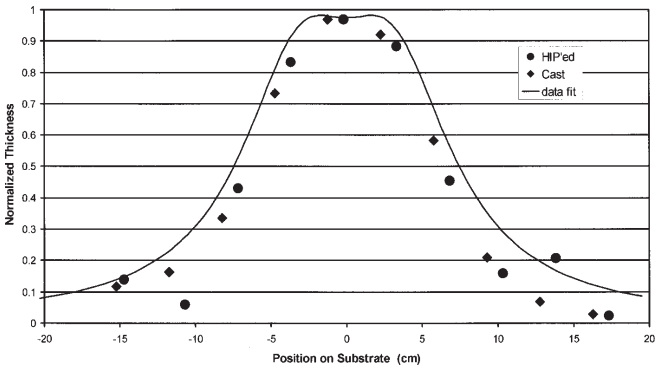

a.

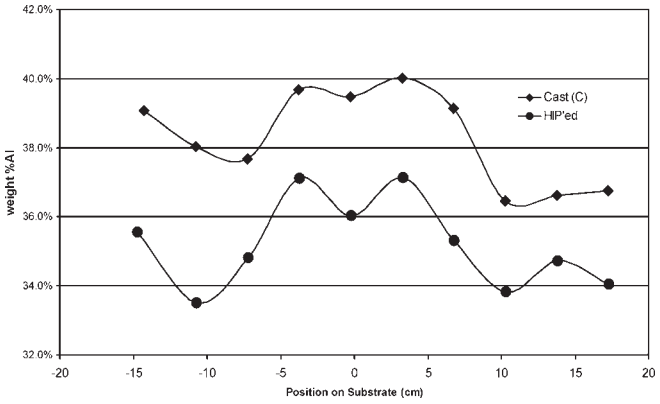

b.

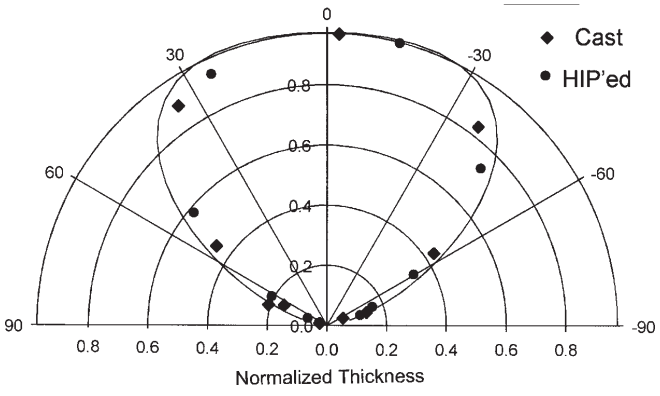

c.

Figure 15: Normalized thickness (a), and weight % Al (b) as a function of position on the substrate, and normalized thickness (c) as a function of the angle θ from the target normal, in polar coordinates. Sputter deposition from the cast and HIP'ed targets was on stationary glass substrates positioned under the target.

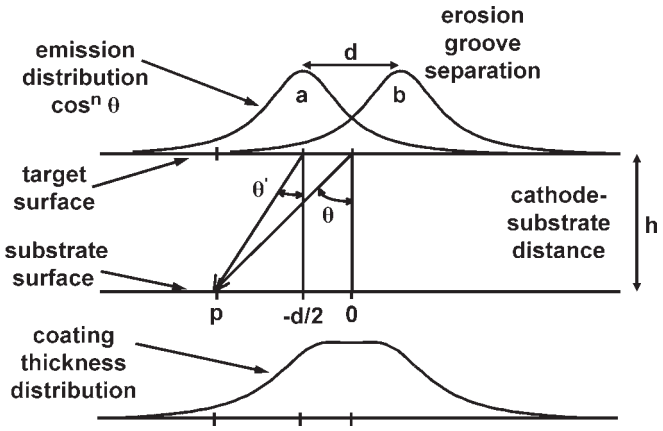

Figure 16: Schematic showing the thickness distribution from two emission sources as a function of the angle θ.

The data in Figure 15a and c were fit by treating the point at the center of the erosion groove from each side of the racetrack (±d/2) as separate emission sources (a and b), and adding together the contribution from each source at point, p, on the substrate, as shown in Figure 16. The emission sources vary as a function of θ', and are located at a distance, d/2, of approximately 3.1 cm from the midpoint between the racetracks. The target substrate distance, h, is approximately 4.8 cm. The erosion grooves were much less than 1 mm deep. The data points for both the cast and HIP'ed targets showed similar distributions, and approximately followed the emission curves shown in Figure 15a and c. The fit for the emission distribution varied as the $\cos^2\theta$ [6], and was peaked more towards the normal than a $\cos\theta$ distribution. A falloff in rate was expected for positions on the substrate greater than about ± 9 cm, since the chamber width is approximately 25 cm.

Figure 15b indicates that coatings deposited from both the cast and HIP'ed targets were not constant in composition across the substrate. Directly below the centerline of the target (located at the point 0), the composition was 36 weight % (50 atomic % Al). The two peaks around the center indicate the concentration of Al deposited below the two racetracks was enriched in Al. The sharp drop-off away from the center is due to the chamber width. The titanium concentration had the opposite behavior, with less concentration under the racetracks and increasing away from the racetrack. Even with the absolute difference in compositions between the targets, the variation in composition with angle is similar between the cast and HIP'ed targets.

A SNMS depth profile of a TiAl coating run at 3 kW is shown in Figure 17. The substrate was passed under the target 10 times at a line speed of 120 inches/min. The Intensity was normalized to the maximum intensity, and the data was smoothed using a moving averages trendline set at a period of 2. The total thickness of the coating was 1640 Å, as calculated from the density. The x-axis shows the sputter time in seconds for the depth profiling, which is proportional to the thickness. To illustrate the periodicity, the gridlines along the x-axis were placed at time intervals equal to the time to sputter etch 164 Å. The SNMS profile indicates the cyclical variation in composition for each pass of the substrate under the target, which is consistent with the nonuniform concentration profile seen with the stationary substrate.

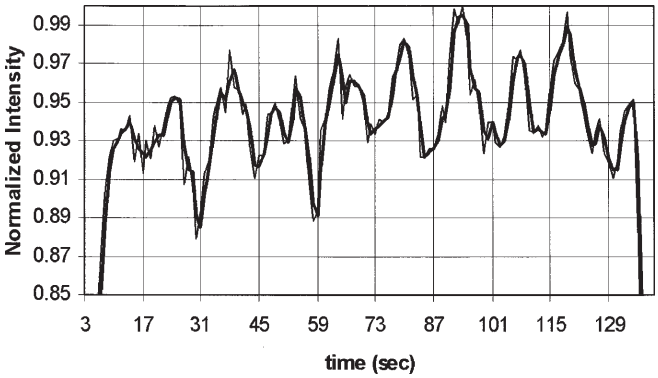

Figure 17: SNMS depth profile of a TiAl coating in terms of the Normalized Intensity as a function of sputter etch time in seconds. The coating was deposited by passing the substrate under the cathode target 10 times.

SUMMARY

Target Microstructure

A HIP'ed target was fabricated from pre-alloyed powder. Cast targets were cut from a TiAl casting to form sputtering surfaces ranging from fine grained to very coarse grained. The HIP'ed target was very fine-grained. The concentrations of Ti and Al of the HIP'ed target agreed with the concentrations of the pre-alloyed powder. However, the concentrations of the cast targets were lower in Ti. The microstructure of the target material was examined and X-ray and powder diffraction patterns of materials ground from the target surfaces confirmed the γ-TiAl phase.

Coating Structure

The structure of the coatings sputtered from the HIP'ed target, and all the cast targets were amorphous as determined from XRD and SAED patterns. This is in agreement with results reported in the literature [7,8] for coatings sputtered from AlTi targets onto various substrates. XRD patterns were obtained for coatings on float glass. TEM micrographs revealed a very fine morphology for the coatings grown on both the carbon support films and NaCl single crystals. HREM images of TiAl coatings on a NaCl substrate, although amorphous, showed evidence of short range order.

Coating Composition and Density

The composition of the coating sputtered from the HIP'ed target (36.1 wt% Al) agreed closely with the target composition (36.2 wt% Al at the center), and the composition of the pre-alloyed powder (36.5 wt% Al) used as the source material for the target. All compositions were in agreement with the specified composition of TiAl. The coating composition sputtered from the cast target (39.1 wt% Al) also closely agreed with the composition of the target (39.5 wt%). However, the composition of the target was 3 wt% over the amount of Al in TiAl. The results for both the cast and HIP'ed targets indicated that there was no loss of either Ti or Al in the coating composition once the target surfaces reached a steady state.

The densities of the coatings sputtered from all the surfaces of the cast targets were approximately equal, but the density of the coatings from the HIP'ed target was slightly greater. This is due to the higher concentration of titanium in the coating sputtered from the HIP'ed versus the cast target.

Deposition Rate

Deposition rates of coatings sputtered from the cast and HIP'ed targets were approximately equal. This was demonstrated by measuring the sputtering rate for the six surfaces in the casting as a function of position, ranging from fine grained at the outer surface to coarse grained at the center. The HIP'ed target was very fine grained. To enhance the effect of erosion on the grain structure, the HIP'ed and coarse-grained targets were sputtered over a period of up to seven hours. Although there is some disagreement in the literature about the effect of grain size on deposition rate [9,10,11], this investigation showed that fine grained and coarse grained targets of the TiAl showed equivalent sputtering rates (9).

Resistivity

Similarly, the resistivities of coatings sputtered from the cast and HIP'ed targets were approximately equal. The values agree with the values for amorphous TiAl films reported in the literature [12,13]. As a comparison, crystalline Ti and Al coatings, deposited from the same ILS coater in a similar manner to the TiAl coatings, have resistivities of 14 and 1.3 μohm-cm, respectively.

Coating Composition and Rate vs. Deposition Angle

The variation in coating thickness and composition as a function of angle from the target surface was determined by sputtering onto a stationary substrate. The data for the coating thickness approximately followed a cosine squared distribution for both the cast and HIP'ed targets, indicating that grain size would not account for any coating nonuniformity. The concentration of Al and Ti in the coating varied as a function of angle from the target, with a higher concentration of Al, the lighter mass element, deposited normal to the direction of the target surface [14], and with a sharp drop-off in concentration at more oblique angles. The converse behavior was true for the Ti concentration. Depth analysis measurements using SNMS verified this variation by showing a periodicity in composition through the depth of the coating for a coating deposited by passing the substrate repeatedly under the target.

CONCLUSION

Cast and HIP'ed targets were characterized. The HIP'ed target showed a very fine grain microstructure with no porosity throughout the whole target. The target composition agreed with the starting material composition of TiAl, which consisted of pre-alloyed powders. The cast targets showed shrinkage porosity, and a variation in grain size ranging from fine near the edges to very coarse in the center. Starting materials of Ti and Al were used for the cast target, and its composition differed from TiAl by up to 3%. The γ-TiAl phase was confirmed for both targets.

Cast targets with grain size ranging from fine to very coarse, and the very fine grained HIP'ed target were DC magnetron sputtered in argon. Under the sputtering conditions outlined in this paper, grain size had no influence on sputtering rate, coating structure, density, resistivity or composition of the coatings. Coating densities were proportional to the concentration of Ti and Al in the targets. The coatings were amorphous with very fine morphology, and showed evidence of short range order. Resistivity agreed with values for amorphous TiAl coatings reported in the literature. Al and Ti concentrations in the coatings agreed with the target concentrations when measured on coatings that were deposited by passing the substrate under the target. However, the concentrations of the coatings varied as a function of angle for coatings deposited on a stationary substrate. A higher concentration of Al was deposited below the racetrack, normal to the direction of the target surface. The variation in coating thickness as a function of angle had an approximately cosine squared distribution. The same behavior was seen for both the cast and HIP'ed targets. The data indicate that there was no difference in the thickness distribution of coatings sputtered from either target.

Although there were no significant differences in the physical properties of the coatings or deposition parameters from either the cast or HIP'ed targets, the HIP'ed target, using prealloyed powder as the source material, should be more consistent and reliable in producing a specified coating composition. In addition, the HIP'ed target was fully dense, whereas the cast target showed porosity, which can lead to problems with arcing, and gas and water absorption, which can jeopardize the coated product and process.

ACKNOWLEDGMENTS

I would like to thank the following associates at PPG Industries, Inc., H. Buhay for his critical reading of the manuscript and valuable input. L. Wagner, V. Frain, E. Goralski,

J. Bowser, P. Snyder, E. Kruppa, and B. Johnson for their analytical work. T. Waynar and J. Benigni for their work in sputter deposition. I would also like to thank U. Habel from Crucibel Industries for her review of the manuscript and input, and T. Nuhfer from Carnegie Mellon University, Pittsburgh, PA, for his input and work on TEM.

REFERENCES

1. D.M. Mattox, "Sputtering Targets," Vacuum Technology & Coating, May 2003, 30; M.T. Willson, "Sputtering Targets: Solid Process Control Starts with the Target," Vacuum Technology & Coating, Mar/Apr. 2000, 8.

2. J.J. Finley, "Heat treatment and bending of low-E glass," Thin Solid Films, 351, (1999), 264.

3. U. Habel, C.F. Yolton, and J. H. Moll, "Gas Atomized g-Titnium Aluminide Base Alloys- Processing, Microstructure and Mechanical Properties," Gamma Titanium Aluminides, Eds. Y.-W. Kim, D.M. Dimiduk, and M.H. Loretto, The Minerals, Metals & Materials Society, 1999, 301-308.

4. The process is further described in JOM, Vol. 52, No 5 May 2000, 23.

5. JCPDS International Center for Diffraction Data, Newtown Square, PA 19073.

6. D.M. Mattox, "Handbook of Physical Vapor Deposition (PVD) Processing," 1st ed., Noyes Publications, Park Ridge, NJ, 1998, p. 326.

7. M. Naka, T. Shibayanagi, M. Maeda, and Y. Ogata, "Formation and physical properties of Ti Based alloys by sputtering," Eds. A. Kobayaski and N.M.Ghoniem, Advances in Applied Plasma Science, Proceedings of the International Symposium on Applied Plasma Science, Los Angeles, (1997), 123.

8. J. F. Sullivan, J. E. Barbier, Y. Lepetitcorps, M. Alnot, and J. J. Ehrhardt, "Chemical and structural analysis of TiAl thin films sputtered deposited on carbon substrates," Surface and Coatings Technology, 61 (1993) 245.

9. C.E. Wickersham, Jr., "Crystallographic target effect in magnetron sputtering," J. Vac. Sci Technol. A, 5(4), 1755, 1987.

10. D.R. Marx, D.P. Strauss, and William Stimson, "The Effect of titanium target grain size on sputtering performance," Materials Research Corporation Advanced, Materials Division Technical Note No. 201, 1993.

11. J.A. Dunlop, J. Yuan, J.K. Kardokus, and R.A. Emigh, U.S. Patent # 5,590,389, "Sputtering Target with Ultra-Fine, Oriented Grains and Methods of Making Same," December 31, 1996.

12. J.H. Moolj, Phys. Stat. Sol., (a) 17, 521 (1973).

13. K.D.D. Rathnayaka, B.D. Hennings, and D.G. Naugle, Phys. Rev. B, 48(10), 6937, (1993).

14. G.K. Wehner, "Sputtering of multicomponent materials," J. Vac. Sci. Technol. A, 1(2), 1983, 487, for a discussion on the angular ejection distribution of different species.